A&A 520, A65 (2010)
DOI: 10.1051/0004-6361/201014943

Astronomy & Astrophysics

Transiting exoplanets from the CoRoT space mission⋆

X. CoRoT-10b: a giant planet in a 13.24 day eccentric orbit

A. S. Bonomo[1], A. Santerne[1,7], R. Alonso[2], J.-C. Gazzano[1,3], M. Havel[3], S. Aigrain[4], M. Auvergne[5], A. Baglin[5], M. Barbieri[21], P. Barge[1], W. Benz[23], P. Bordé[6], F. Bouchy[7,8], H. Bruntt[5], J. Cabrera[9,19], A. C. Cameron[22], L. Carone[10], S. Carpano[11], Sz. Csizmadia[9], M. Deleuil[1], H. J. Deeg[12], R. Dvorak[13], A. Erikson[9], S. Ferraz-Mello[14], M. Fridlund[11], D. Gandolfi[11,15], M. Gillon[16], E. Guenther[15], T. Guillot[3], A. Hatzes[15], G. Hébrard[8], L. Jorda[1], H. Lammer[17], A. F. Lanza[20], A. Léger[6], A. Llebaria[1], M. Mayor[2], T. Mazeh[18], C. Moutou[1], M. Ollivier[6], M. Pätzold[10], F. Pepe[2], D. Queloz[2], H. Rauer[9,24], D. Rouan[5], B. Samuel[6], J. Schneider[19], B. Tingley[12], S. Udry[2], and G. Wuchterl[15]

(Affiliations can be found after the references)

Received 5 May 2010 / Accepted 10 June 2010

ABSTRACT

Context. The space telescope CoRoT searches for transiting extrasolar planets by continuously monitoring the optical flux of thousands of stars in several fields of view.

Aims. We report the discovery of CoRoT-10b, a giant planet on a highly eccentric orbit ($e = 0.53 \pm 0.04$) revolving in 13.24 days around a faint ($V = 15.22$) metal-rich K1V star.

Methods. We used CoRoT photometry, radial velocity observations taken with the *HARPS* spectrograph, and *UVES* spectra of the parent star to derive the orbital, stellar, and planetary parameters.

Results. We derive a radius of the planet of $0.97 \pm 0.07\ R_{\rm Jup}$ and a mass of $2.75 \pm 0.16\ M_{\rm Jup}$. The bulk density, $\rho_{\rm p} = 3.70 \pm 0.83$ g cm^{-3}, is ∼2.8 that of Jupiter. The core of CoRoT-10b could contain up to 240 $M_\oplus$ of heavy elements.

Moving along its eccentric orbit, the planet experiences a 10.6-fold variation in insolation. Owing to the long circularisation time, $\tau_{\rm circ} > 7$ Gyr, a resonant perturber is not required to excite and maintain the high eccentricity of CoRoT-10b.

Key words. stars: fundamental parameters – techniques: photometric – techniques: radial velocities – techniques: spectroscopic

1. Introduction

CoRoT is the pioneer space mission dedicated to detecting extrasolar planets via the transit method (Baglin 2003; see Auvergne et al. 2009 for a detailed description of the instrument and its performance). To date it has led to the discovery of ten extrasolar planets: CoRoT-7b, the first superEarth with measured radius and mass (Léger et al. 2009; Queloz et al. 2008); three inflated hot Jupiters: CoRoT-1b (Barge et al. 2008), CoRoT-2b (Alonso et al. 2008a), and CoRoT-5b (Rauer et al. 2009); CoRoT-3b, "the first secure inhabitant of the brown dwarf desert" (Deleuil et al. 2008); two Jupiter-like planets with an orbital period of approximately 9 days: CoRoT-4b (Aigrain et al. 2008; Moutou et al. 2008) and CoRoT-6b (Fridlund et al. 2010); the hot sub-Saturn CoRoT-8b (Bordé et al. 2010); and the long-period temperate giant planet CoRoT-9b (Deeg et al. 2010).

Here we report the discovery of the giant planet CoRoT-10b that orbits its parent star in 13.24 days, moving along a highly eccentric orbit with $e = 0.53 \pm 0.04$. It is therefore one of the few known transiting planets with $e \gtrsim 0.5$, such as HD 147056b (alias HAT-P-2b, $e = 0.52$ and orbital period $P = 5.63$ days; Bakos et al. 2007; Pál et al. 2010), HD 17156b ($e = 0.67$ and $P = 21.22$ days; Barbieri et al. 2007, 2009) and HD 80606b ($e = 0.93$ and $P = 111.44$ days; Moutou et al. 2009; Winn et al. 2009; Hébrard et al. 2010). Eccentric transiting planets include those with lower eccentricity, notably the recently discovered WASP-8b ($e = 0.31$ and $P = 8.16$ days; Queloz et al. 2010) and HAT-P-15b ($e = 0.19$ and $P = 10.9$ days; Kovács et al. 2010), the massive planet X0-3b ($e = 0.26$ and $P = 3.19$ days; Johns-Krull et al. 2008; Winn et al. 2008), and the two Neptunes: GJ 436b ($e = 0.15$ and $P = 2.64$ days; Gillon et al. 2007a,b; Alonso et al. 2008b; Bean et al. 2008) and HAT-P-11b ($e = 0.20$ and $P = 4.89$ days; Bakos et al. 2010).

Transiting planets in eccentric orbits are very intriguing and interesting objects as they allow us to study ongoing tidal dissipation and its impact on the planet radius (Ibgui et al. 2010), atmospheric circulation in the case of a strong variation in insolation (Langton & Laughlin 2007), the dynamical orbital evolution including the gravitational interaction between planets in a multiple system (planet-planet scattering; e.g., Marzari & Weidenschilling 2002), or the secular influence of a possible distant stellar companion (Kozai mechanism; Kozai 1962).

2. CoRoT observations

The parent star of CoRoT-10b, i.e. the CoRoT target LRc01_E2_1802, is a $V = 15.22$ star and has been observed in the stellar field pointing towards the constellation of Aquila during the first CoRoT long run LRc01 (Cabrera et al. 2009). Its magnitudes in several photometric bands and its coordinates are reported in Table 1. CoRoT observations of this target lasted

⋆ The CoRoT space mission, launched on December 27th 2006, has been developed and is operated by CNES, with the contribution of Austria, Belgium, Brazil, ESA (RSSD and Science Programme), Germany and Spain.

Table 1. CoRoT-10 IDs, coordinates, and magnitudes.

CoRoT window ID	LRc01_E2_1802	
CoRoT ID	100725706	
USNO-A2 ID	0900-14919216	
2MASS ID	19241528+0044461	
GSC2.3 ID	NIMR021985	
Coordinates		
RA (J2000)	19:24:15.29	
Dec (J2000)	00:44:46.11	
Magnitudes		
Filter	Mag	Error
B^a	16.68	0.14
V^a	15.22	0.05
r'^a	14.73	0.03
i'^a	13.74	0.03
J^b	12.53	0.02
H^b	11.93	0.03
K^b	11.78	0.02

Notes. [(a)] Provided by Exo-Dat (Deleuil et al. 2009); [(b)] from 2MASS catalogue.

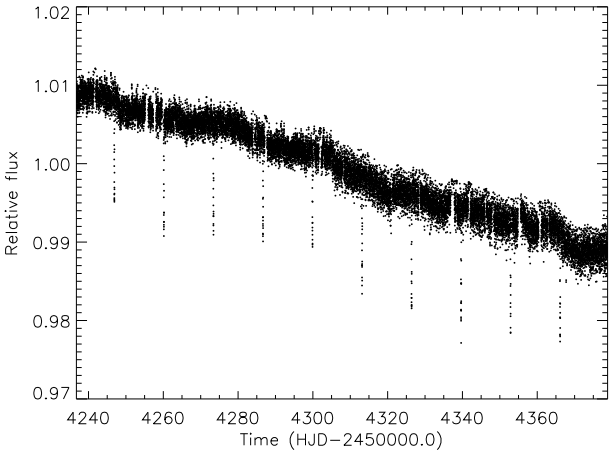

Fig. 1. The quiescent light curve of CoRoT-10 binned at 512 s showing ten transits of the giant planet CoRoT-10b. Jumps due to hot pixels were removed by means of an iterative 3-sigma clipping.

for 142.07 days, from 16 May up to 15 October 2007, and provided us with monochromatic (white channel) data (Auvergne et al. 2009).

Transits by CoRoT-10b were first discovered in "alarm mode" (Surace et al. 2008), i.e. while CoRoT observations were still ongoing, which permitted us to change the temporal sampling from 512 s to 32 s after HJD 2 454 305.11. In total, 210 248 photometric measurements were obtained, 198 752 in the 32 s oversampling mode[1]. Figure 1 shows the CoRoT-10 light curve with the nominal sampling of 512 s, filtered from a) outliers that are produced by proton impacts during the crossing of the South Atlantic Anomaly of the Earth's magnetic field by the satellite; and b) several jumps, with a typical duration shorter than 1 day, due to hot pixels. Corrections for the CCD zero offset, sky background, Earth's scattered light and jitter variations were carried out by the latest version 2.1 of the CoRoT reduction pipeline. Unlike CoRoT-2 (Lanza et al. 2009), CoRoT-6 (Fridlund et al. 2010), and CoRoT-7 (Lanza et al. 2010), the light

[1] Data available at http://idoc-corot.ias.u-psud.fr/.

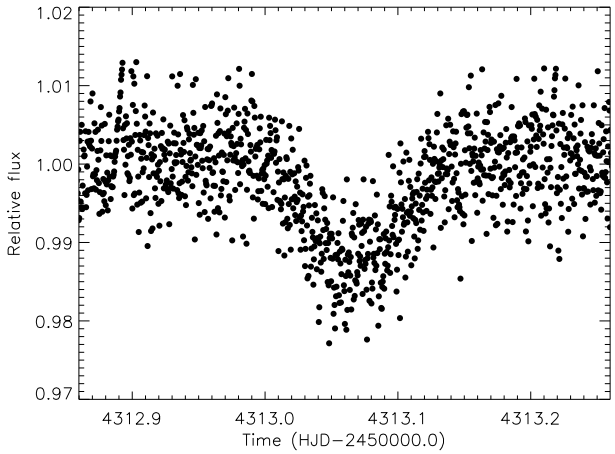

Fig. 2. One of the five 32 s oversampled transits of CoRoT-10b.

curve of CoRoT-10 is relatively quiescent and does not show flux variations due to the presence of starspots and photospheric faculae greater than a few mmag. It shows a long term decrease of ∼2.5% attributable to CCD ageing (Fig. 1). The rms of the nominal and oversampled photometric points is 0.0013 and 0.0046 in relative flux units, respectively.

A total of 10 transits with a depth of ∼1.3% are visible in the light curve (Fig. 1). A zoom of one of the five 32 s oversampled transits is shown in Fig. 2. The transit ephemeris, reported in Table 4, was derived from a linear fit to the measured transit mid points determined by a trapezoidal fitting of each transit. It gives an orbital period of 13.2406 ± 0.0002 days.

3. Ground-based follow-up observations

3.1. Radial velocity observations

We performed radial velocity (*RV*) observations of the star CoRoT-10 with the *HARPS* spectrograph (Pepe et al. 2002b, Mayor et al. 2003) at the 3.6-m ESO telescope (La Silla, Chile). *HARPS* was used with the observing mode obj_AB, without acquiring a simultaneous Thorium lamp spectrum in order to monitor the Moon background light on the second fibre. The intrinsic stability of this spectrograph does not require the use of lamp-calibration spectra, because the instrumental drift during one night is in our case always smaller than the stellar *RV* photon noise uncertainties. *HARPS* data were reduced with the online standard pipeline, and radial velocities were obtained by a weighted cross-correlation with a numerical spectral mask for a K5V star (Baranne 1996; Pepe et al. 2002a).

The first two measurements of CoRoT-10 were made in June 2008[2]. Seventeen additional measurements were obtained from June to September 2009[3]. Seven of our nineteen measurements were strongly contaminated by the moonlight, i.e. the radial velocity of the Moon was close to that of CoRoT-10 and affected both the *RV* measurements and the bisector lines. We developed a software correction using the Moon spectrum simultaneously acquired on fibre B: it consists in subtracting the cross-correlation function (CCF) of fibre B, containing the Sun spectrum (reflected by the Moon), from the CCF of fibre A, containing the stellar spectrum. The correction was applied when

[2] *HARPS* program 081.C-0388.
[3] *HARPS* program 083.C-0186.

Table 2. Radial velocity measurements of CoRoT-10 obtained by *HARPS*.

HJD[a] −2 400 000	*RV* [km s^{-1}]	$\pm1\sigma$ [km s^{-1}]	BIS [km s^{-1}]	Exp. time [s]	S/N/pix. (at 550 nm)
54 640.85815[b]	15.386	0.038	0.021	3600	7.4
54 646.74608	15.049	0.035	0.087	1800	5.1
54 986.78569[b]	15.322	0.049	0.081	3600	4.5
54 989.77932[b]	14.947	0.035	–0.048	3600	9.2
54 990.81302[b]	14.923	0.038	0.004	3600	7.1
54 994.81853[b]	15.545	0.036	–0.014	3600	8.4
54 995.80369[b]	15.479	0.032	–0.050	3600	10.8
55 022.79584[b]	15.503	0.035	0.015	3600	7.0
55 063.69761	15.507	0.032	0.055	3300	5.4
55 068.67093	15.079	0.018	–0.024	3600	7.7
55 069.68356	14.947	0.019	0.006	3300	7.6
55 070.69173	15.146	0.021	0.070	3000	7.4
55 071.51030	15.414	0.019	–0.074	3000	7.8
55 072.54251	15.456	0.020	–0.014	3000	7.5
55 073.57439	15.492	0.015	–0.030	3000	9.1
55 074.61800	15.508	0.022	–0.073	3600	7.7
55 075.53585	15.468	0.029	–0.018	3000	6.4
55 077.62048	15.398	0.032	0.114	3000	5.7
55 078.61399	15.343	0.024	0.018	3600	7.6

Notes. [(a)] Heliocentric Julian Date;
[(b)] exposures affected by the moonlight with 30 m s^{-1} quadratically added to their errors.

the two CCF peaks were close in radial velocity. For CoRoT-10, corrections in the range between 50 and 550 m s^{-1} were applied for seven measurements. To be conservative, we added quadratically 30 m s^{-1} of systematic errors to these seven corrected measurements.

The radial velocities are listed in Table 2 and displayed in Figs. 3 and 4. The phase-folded radial velocity curve shows a variation in phase with the CoRoT transit period. It is compatible with the reflex motion of the parent star due to an eccentric planetary companion. We fitted the data with a Keplerian orbit using the CoRoT ephemeris P = 13.2406 days and $T_{\rm tr}$ = 2 454 273.3436 HJD (see Table 4). The derived eccentricity and argument of periastron are e = 0.53 ± 0.04 and ω = 218.9 ± 6.4 deg. The other orbital parameters are reported in Table 4. The standard deviation of the residuals to the fit σ(O−C) = 29 m s^{-1} is comparable to the mean RV uncertainty.

To examine the possibility that the RV variation is the result of a blended binary scenario – a single star with an unresolved and diluted eclipsing binary –, we followed the procedure described in Bouchy et al. (2008) based on checking both the spectral line asymmetries and the dependencies of the RV variations on different cross-correlation masks. These two checks excluded the RV variation being caused by a blended binary and allowed us to establish the planetary nature of CoRoT-10b. The bisector variations are shown in Fig. 5.

3.2. Photometric observations

Photometric observations during and outside the transit were carried out at the 1.20 m telescope of the Observatoire de Haute Provence during the nights of 18 June and 15 July 2009, respectively. Such observations are complementary to the radial velocity measurements and are required to definitively exclude the possibility that the transits detected in the CoRoT light curve could be produced by a background eclipsing binary that contaminates the CoRoT aperture mask of the star (Deeg et al. 2009). The latter covers ∼16″ × 14″ on the sky and contains two

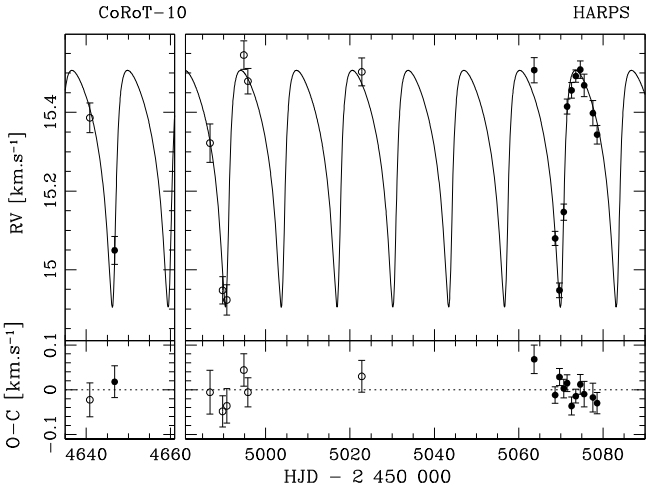

Fig. 3. *Top panel*: radial velocity measurements and the Keplerian best-fit solution (solid line). *Bottom panel*: residuals from the best fit. The open circles indicate the measurements affected by the moonlight after our correction.

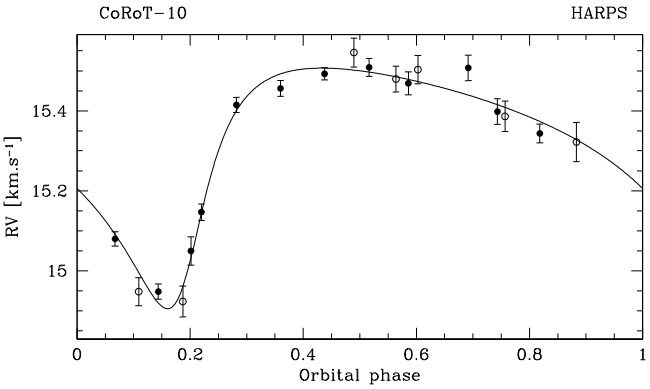

Fig. 4. Phase-folded radial velocity curve of CoRoT-10 and the Keplerian best-fit solution (solid line). The open circles indicate the measurements affected by the moonlight after our correction.

main background contaminants: one is 3.78 mag fainter in V and is located at ∼6.5″ from CoRoT-10 toward the south west; the other one is 4.22 mag fainter in V and is ∼7.5″ toward the north east (see Fig. 6). Differential photometry shows an "on-target" transit with the same depth as observed in the CoRoT light curve. None of the two contaminants exhibits significant flux variations that can mimic the transits observed in the CoRoT-10 light curve.

4. Transit fitting

For the transit fitting, we first filtered the raw light curve from outliers due to impacts of cosmic rays. Based on pre-launch observations stored in the Exo-Dat catalogue (Deleuil et al. 2009), we estimated the flux contamination from the two faint background stars that fall inside the CoRoT-10 photometric mask to be 5.5 ± 0.3% (see Fig. 6). We subtracted such a value from the median flux of the light curve (75 559 e$^-$/32 s), which makes the transits slightly deeper by ∼7 × 10^{-4} in relative flux. We then fitted a parabola to the 5 h intervals of the light curve before the ingress and after the egress of each transit to correct for any local variations. We disregarded two of the ten CoRoT-10b transits, precisely the second transit and the ninth, as their shape was deformed by hot pixels. Finally, we folded the light curve using the ephemeris reported in Table 4 and binning the data points in

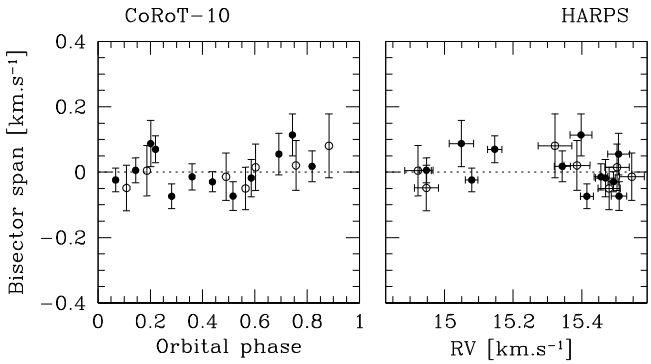

Fig. 5. Bisector variations (span of the bisector slope) as a function of orbital phase (*left pannel*) and radial velocity (*right pannel*). Bisector error bars are estimated as twice the radial velocity uncertainties. No bisector effect is visible for the moonlight-corrected measurements (open circles) indicating the good quality of our correction.

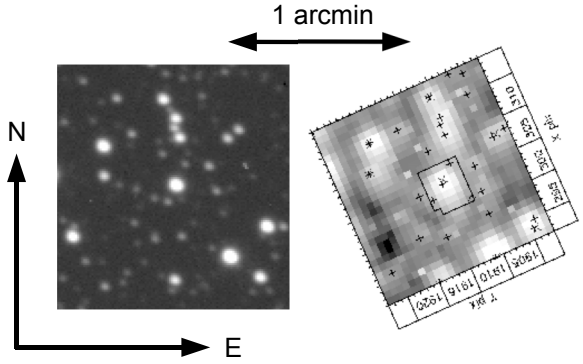

Fig. 6. The sky area around CoRoT-10 (the brightest star near the centre). *Left*: *R*-filter image with a resolution of ~2.5″ taken with the OHP 1.20 m telescope. *Right*: image taken by CoRoT, with the same scale and orientation. The jagged outline in its centre is the photometric aperture mask; also indicated are CoRoT's x and y image coordinates and position of nearby stars from the Exo-Dat database (Deleuil et al. 2009).

bins of 8×10^{-5} in phase, corresponding to ~1.5 min (Fig. 7). The error on each bin was computed as the standard error of the data points inside the bin.

Transit best fit was performed following the formalism of Giménez (2006, 2009) and fixing the eccentricity and the argument of the periastron to the values derived from the Keplerian fit of the radial velocity measurements (see Sect. 3.1). The four free parameters of the transit model are the transit centre; the phase of the end of transit egress θ_2 in the reference system for eccentric orbits defined by Giménez & Garcia-Pelayo (1983) and shown in their Fig. 1 (see also Giménez 2009); the ratio of the planet to stellar radii $k = R_p/R_*$; and the inclination i between the orbital plane and the plane of the sky. The two non-linear limb-darkening coefficients $u_+ = u_a + u_b$ and $u_- = u_a - u_b$[4] were fixed for two reasons: first, the relatively low signal-to-noise ratio of the transit light curve, which does not allow us to constrain either u_+ or u_- within reasonable error bars; second, the degeneracy between the inclination and the two limb darkening coefficients in the case of a high impact parameter b, as in our case $b = 0.85 \pm 0.03$ (see Table 4). The adopted limb-darkening coefficients u_a and u_b for the CoRoT bandpass were determined following the procedure in Sing (2010). However, while the latter only takes the stellar emergent intensity into account for the values of $\mu \geq 0.05$, we considered all the 17 values available in the ATLAS model grids[5] down to $\mu = 0.01$. Our choice is motivated by the grazing transit of CoRoT-10b, which implies that the variation in the specific intensity close to the limb of the stellar disc must be considered properly when modelling the transit shape. The derived limb-darkening quadratic coefficients are $u_a = 0.51$ and $u_b = 0.21$, which give $u_+ = 0.72$ and $u_- = 0.3$.

The best-fit transit parameters were found by using the algorithm AMOEBA (Press et al. 1992) and changing the initial values of the parameters with a Monte-Carlo method to find the global minimum of the χ^2. Our best fit of the phase-folded and binned transit light curve is shown in Fig. 7. Fitted and derived transit parameters are listed in Table 4 together with their 1-sigma errors estimated using the bootstrap procedure described in Alonso et al. (2008a) which takes also the correlated noise into account (cf. Alonso et al. 2008a, Sect. 3). Uncertainties on the eccentricity, the argument of the periastron and the contamination were also considered for estimating the errors of the derived transit parameters b, a/R_*, a/R_p, $M_*^{1/3}/R_*$ and ρ_*, where b is the impact parameter, a the semi-major axis of the planetary orbit, R_* and M_* the stellar radius and mass, R_p the planet radius, and ρ_* the stellar density (see Table 4). The fitted value of the transit centre is consistent with zero within 1-sigma, which confirms the good quality of the transit ephemeris (Sect. 2).

5. Stellar and planetary parameters

The spectral analysis of the parent star was performed with a high-resolution *UVES* spectrum acquired on 30 July 2009[6]. We used the Dic1 mode (390+580) and a slit width of 0.8″, achieving a resolving power of ~55 000. The total exposure time was 4 h leading to a signal-to-noise ratio per pixel $S/N \sim 120$ at 5500 Å.

To derive the stellar atmospheric parameters, we first determined the $V \sin i_* = 2 \pm 0.5\,\mathrm{km\,s^{-1}}$. We selected a few *HARPS* spectra that were not contaminated by the Moon reflected light. This series of spectra was set at rest and co-added. To carry out the detailed spectral analysis, we made use of the *VWA* (Bruntt 2009) software package and obtained: $T_{\rm eff} = 5075 \pm 75$ K, $\log g = 4.65 \pm 0.10$ cm s^{-2}, and [Fe/H] $= 0.26 \pm 0.07$ dex. The surface gravity value was checked with usual indicators: Na I D lines around 5890 Å, Mg I b lines, and Ca I lines at 6122, 6162, and 6439 Å. The abundances of several chemical elements are listed in Table 3. The elements for which we could only measure a few lines are not reported. The absence of noticeable emission in the core of the Ca II H & K lines supports the low magnetic activity of CoRoT-10 indicated by its quiescent light curve (see Fig. 1).

Saturated interstellar Na D lines in the *HARPS* spectra indicate a significant absorption along the line of sight. Converting the 2MASS J and K magnitudes (Table 1) in the Bessel & Brett

[4] u_a and u_b are the coefficients of the limb-darkening quadratic law: $I(\mu)/I(1) = 1 - u_a(1-\mu) - u_b(1-\mu)^2$, where $I(1)$ is the specific intensity at the centre of the disc and $\mu = \cos\gamma$, γ being the angle between the surface normal and the line of sight.

[5] http://kurucz.harvard.edu

[6] *UVES* program ID: 083.C-0690(A).

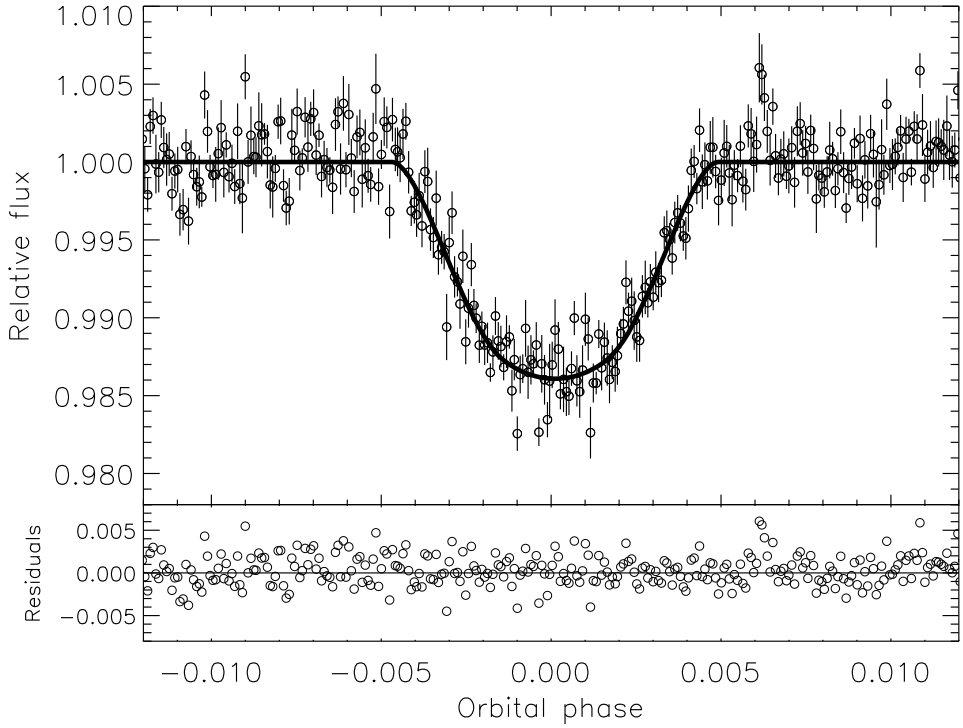

Fig. 7. *Top panel*: phase-folded light curve of 8 transits of CoRoT-10b. The bin size corresponds to 1.5 min and the 1-sigma error bars on each bin are estimated as the standard error of the data points inside the bin. The solid line shows our best-fit transit model. *Bottom panel*: the residuals from the best-fit model.

Table 3. Abundances of some chemical elements for the fitted lines in the *UVES* spectrum.

Element	$[X/H]$	Number of lines
Ca I	0.21 ± 0.12	5
Ti I	0.38 ± 0.11	15
V I	0.63 ± 0.12	10
Cr I	0.34 ± 0.13	7
Fe I	0.26 ± 0.10	77
Fe II	0.26 ± 0.11	5
Co I	0.41 ± 0.10	7
Ni I	0.35 ± 0.10	23
Si I	0.37 ± 0.10	8

photometric system (Bessell & Brett 1988), and comparing the $(J-K)$ colour with what is expected by Kurucz models for the CoRoT-10 spectral type and metallicity, we found a colour excess $E(J-K) \simeq 0.24$. This corresponds to an extinction of $A_V \simeq 1.39$ mag[7], in agreement with reddening maps (Schlegel et al. 1998). Using the Pogson formula[8], the stellar distance was estimated to 345 ± 70 pc.

From the transit best fit we derived a stellar density of $\rho_* = 3.32 \pm 0.70$ g cm^{-3}, i.e., $2.35 \pm 0.50\ \rho_\odot$. CESAM (Morel 2008) and STAREVOL (Palacios, private communication; Siess 2006) models of stellar evolution do not foresee any evolutionary track that matches the above-mentioned stellar density, given the effective temperature and the metallicity of CoRoT-10. Specifically, they predict an upper limit of 2.55 g cm^{-3} ($1.79\,\rho_\odot$), compatible at 1.1-sigma with the stellar density derived from the transit fitting. The mass and radius of the star provided by the CESAM evolutionary tracks are respectively equal to $M_* = 0.89 \pm 0.05\ M_\odot$ and $R_* = 0.79 \pm 0.05\ R_\odot$. The corresponding surface gravity, $\log g = 4.59 \pm 0.06$ cm s^{-2}, is in good agreement with the spectroscopic value. The stellar age constraints are relatively weak but favour values lower than 3 Gyr.

From the aforementioned stellar radius and mass, we determined the radius of the planet $R_\mathrm{p} = 0.97 \pm 0.07\ R_\mathrm{Jup}$ and its mass $M_\mathrm{p} = 2.75 \pm 0.16\ M_\mathrm{Jup}$. The bulk density, $\rho_\mathrm{p} = 3.70 \pm 0.83$ g cm^{-3}, is ~2.8 that of Jupiter.

6. Discussion and conclusions

We have reported the discovery of CoRoT-10b, a transiting planet on a highly eccentric orbit ($e = 0.53 \pm 0.04$) with a mass of $2.75 \pm 0.16\ M_\mathrm{Jup}$ and a radius of $0.97 \pm 0.07\ R_\mathrm{Jup}$. It orbits a metal-rich ([Fe/H] $= 0.26 \pm 0.07$) K1V star with a visual magnitude $V = 15.22$ in 13.24 days. Figure 8 shows the position of CoRoT-10b in the eccentricity-period diagram of the known extrasolar planets and highlights its peculiarity, because it belongs to the class of the few transiting exoplanets with highly eccentric orbits ($e \gtrsim 0.5$) among which are HAT-P-2b, HD 17156b, and HD 80606b.

To investigate the internal structure of CoRoT-10b, we computed planetary evolution models with CEPAM (Guillot & Morel 1995) under the standard hypothesis that the planet is made up of a central rocky core of variable mass and of an overlying envelope of solar composition (e.g., Guillot 2008). The results in terms of planetary size as a function of system age are shown in Fig. 9. The coloured regions (red, blue, yellow-green) indicate the constraints derived from the stellar evolution models at 1, 2, and 3σ level, respectively. Assuming a zero Bond albedo, we derived the equilibrium temperature of the planet $T_\mathrm{eq} = 600$ K. For this temperature, models of planet

[7] $A_V/E(J-K) = 5.82 \pm 0.1$ (Cox 2000).

[8] $V - M_V = 5 \log d - 5 + A_V$, where M_V was determined from the bolometric magnitude, given the T_eff and R_* of CoRoT-10, and the BC taken from http://kurucz.harvard.edu for the atmospheric parameters of CoRoT-10.

Table 4. Planet and star parameters.

Ephemeris	
Planet orbital period P [days]	13.2406 ± 0.0002
Planetary transit epoch $T_{\rm tr}$ [HJD-2 400 000]	54 273.3436 ± 0.0012
Planetary transit duration $d_{\rm tr}$ [h]	2.98 ± 0.06
Planetary occultation epoch $T_{\rm occ}$[a] [HJD-2 400 000]	54 276.49 ± 0.41
Planetary occultation duration $d_{\rm occ}$ [h]	2.08 ± 0.18
Epoch of periastron T_0 [HJD-2 400 000]	54 990.85 ± 0.08
Derived parameters from radial velocity observations	
Orbital eccentricity e	0.53 ± 0.04
Argument of periastron ω [deg]	218.9 ± 6.4
Radial velocity semi-amplitude K [m s^{-1}]	301 ± 10
Systemic velocity $V_{\rm r}$ [km s^{-1}]	15.330 ± 0.007
O−C residuals [m s^{-1}]	29
Fitted and fixed transit parameters	
θ_2[b]	0.00483 ± 0.00009
Radius ratio $k = R_{\rm p}/R_*$	0.1269 ± 0.0038
Inclination i [deg]	88.55 ± 0.2
u_+ (fixed)	+0.72
u_- (fixed)	+0.30
Derived transit parameters	
a/R_*[c]	31.33 ± 2.15
$a/R_{\rm p}$	247 ± 21
$(M_*/M_\odot)^{1/3}(R_*/R_\odot)^{-1}$	1.33 ± 0.09
Stellar density ρ_* [g cm^{-3}]	3.32 ± 0.70
Impact parameter b[d]	0.85 ± 0.03
Spectroscopic parameters of the star	
Effective temperature $T_{\rm eff}$[K]	5075 ± 75
Surface gravity log g [cgs]	4.65 ± 0.10
Metallicity [Fe/H] [dex]	+0.26 ± 0.07
Stellar rotational velocity $V \sin i_*$ [km s^{-1}]	2.0 ± 0.5
Spectral type	K1V
Stellar and planetary physical parameters	
Star mass [$M_\odot$][e]	0.89 ± 0.05
Star radius [$R_\odot$][e]	0.79 ± 0.05
Planet mass $M_{\rm p}$ [$M_{\rm Jup}$]	2.75 ± 0.16
Planet radius $R_{\rm p}$ [$R_{\rm Jup}$]	0.97 ± 0.07
Planet density $\rho_{\rm p}$ [g cm^{-3}]	3.70 ± 0.83
Planet surface gravity log $g_{\rm p}$ [cgs]	3.93 ± 0.08
Planet rotation period $P_{\rm p,rot}$ [days][f]	4.25 ± 0.53
Distance of the star d [pc]	345 ± 70
Orbital semi-major axis a [AU]	0.1055 ± 0.0021
Orbital distance at periastron $a_{\rm per}$ [AU]	0.0496 ± 0.0039
Orbital distance at apoastron $a_{\rm apo}$ [AU]	0.1614 ± 0.0047
Equilibrium temperature at the averaged distance $T_{\rm eq}$ [K][g]	600 ± 23
Equilibrium temperature at periastron $T_{\rm eq}^{\rm per}$ [K][g]	935 ± 54
Equilibrium temperature at apoastron $T_{\rm eq}^{\rm apo}$ [K][g]	518 ± 20

Notes. [(a)] $T_{\rm occ} = T_{\rm tr} + \frac{P}{\pi} \cdot \left(\frac{\pi}{2} + (1 + \csc^2 i) \cdot e \cos\omega\right)$;
[(b)] phase of the end of transit egress in the reference system defined by Giménez & Garcia-Pelayo (1983);
[(c)] $a/R_* = \frac{1+e\cdot\cos\nu_2}{1-e^2} \cdot \frac{1+k}{\sqrt{1-\cos^2(\nu_2+\omega-\frac{\pi}{2})\cdot\sin^2 i}}$, where ν_2 is the true anomaly measured from the periastron passage at the end of transit egress (see Giménez 2009);
[(d)] $b = \frac{a\cdot\cos i}{R_*} \cdot \frac{1-e^2}{1+e\cdot\sin\omega}$;
[(e)] from CESAM stellar evolution models. See Sect. 5 for details;
[(f)] assuming the planet to be in a pseudo-synchronous rotation;
[(g)] black body equilibrium temperature for an isotropic planetary emission.

internal structure with a core mass of 0, 20, 60, 120, 180, 240, and 320 $M_\oplus$ were computed (Fig. 9). A 25% change in the equilibrium temperature yields a difference in the resulting planetary radius of less than 1%. Therefore, a Bond albedo $A_{\rm B}$ that is considerably greater than zero (up to $A_{\rm B} = 0.7$) does not change our results significantly.

CoRoT-10b is a high density planet with a mass and density similar to those of HD 17156b (Barbieri et al. 2009) but with a higher content of heavy elements. For an age of the star, hence of the planetary system between 1 and 3 Gyr, CoRoT-10b should contain between 120 and 240 $M_\oplus$ of rocks in its interior (i.e. between 14 and 28% of the total mass), at 1-sigma level. Mixing

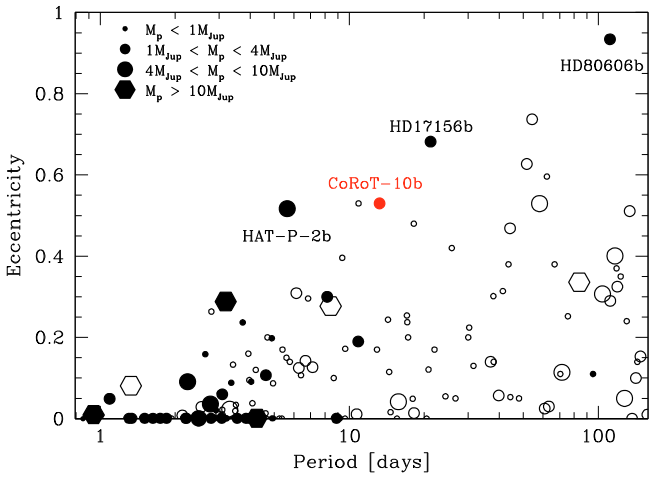

Fig. 8. Eccentricity – period diagram for the known extrasolar planets (black filled symbols are transiting planets). The size of the symbol indicates the mass range. CoRoT-10b, with P = 13.24 days and e = 0.53, is indicated by the red filled circle. Data from http://exoplanet.eu.

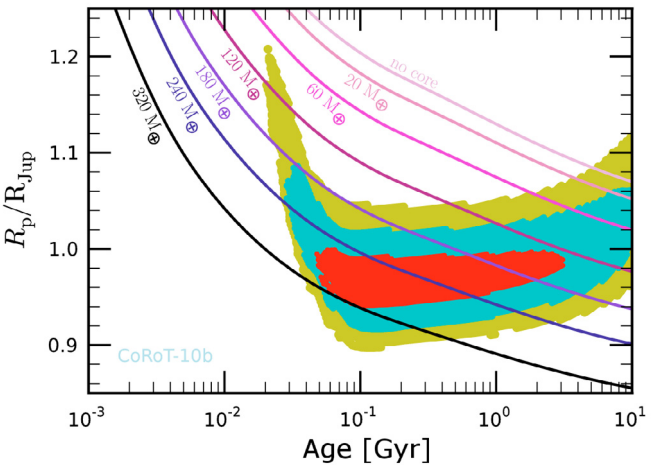

Fig. 9. Evolution of the radius of CoRoT-10b (in Jupiter units) as a function of age, compared to constraints inferred from CoRoT photometry, spectroscopy, radial velocimetry, and CESAM stellar evolution models. Red, blue, and green areas correspond to the planetary radii and ages that result from stellar evolution models matching the inferred $\rho_* - T_{\rm eff}$ uncertainty ellipse within 1σ, 2σ, and 3σ, respectively. Planetary evolution models for a planet with a solar-composition envelope over a central dense core of pure rocks of variable mass are shown as solid lines. These models assume a total mass of 2.75 $M_{\rm Jup}$ and an equilibrium temperature of 600 K (corresponding to a zero Bond albedo). They depend weakly on the assumed opacities, and the uncertainties due to the atmospheric temperature and planetary mass are negligible.

heavy elements in the envelope rather than assuming that they are all contained in the core may yield a reduction of these numbers by ∼30% (Baraffe et al. 2008). This number is uncertain, however, because it does not account for the increase in opacity in the outer radiative zone that would have the opposite effect (Guillot 2005). In any case, CoRoT-10b is found to be extremely enriched in heavy elements, suggesting that its formation probably required giant collisions (see Ikoma et al. 2006). It also strengthens the observed correlation between star metallicity and heavy elements in the planet (Guillot 2008).

Moving along its eccentric orbit from the periastron to the apoastron, CoRoT-10b experiences a 10.6-fold variation in insolation. Moreover, since the tidal interaction with the parent star is strongest around periastron, the planet is expected to be in pseudo-synchronous rotation. Equation (42) from Hut (1981) gives a rotation period of the planet $P_{\rm p,rot} = 4.25 \pm 0.53$ days. Time-dependent radiative models of planetary atmospheres could be used both to study heating variations from the changing star-planet distance at different pressure levels of the planet atmosphere and to predict temperature inversions caused by strong heating around periastron, as done by Iro & Deming (2010) for HD 17156b and HD 80606b.

Using Eq. (6) in Matsumura et al. (2008), we can estimate the circularisation time $\tau_{\rm circ}$ of the planetary orbit, neglecting the stellar damping. The circularisation time strongly depends on the adopted tidal quality factor for the planet $Q'_{\rm p}$, which is not well known. For Jupiter, $5 \times 10^4 < Q'_{\rm p} < 2 \times 10^6$ (Yoder & Peale 1981; Lainey et al. 2009), and for most of the giant extrasolar planets $10^5 < Q'_{\rm p} < 10^9$ (see Fig. 2 from Matsumura et al. 2008). Considering $Q'_{\rm p} = 10^5$, we find $\tau_{\rm circ} \sim 7.4$ Gyr. Owing to the long circularisation time, the eccentricity of CoRoT-10b need not be excited and maintained by the resonant interaction with another planet. Nevertheless, the eccentric orbits of extrasolar planets can be explained by gravitational planet-planet scattering (e.g., Chatterjee et al. 2008, and references therein). If another massive planet survived the violent encounters between planets and is currently orbiting the parent star, it could be detected by a long-term radial-velocity follow-up of the parent star, e.g., showing a long-term drift induced by the distant companion. If the star has a distant companion of stellar nature, the high eccentricity of CoRoT-10b could be produced by Kozai oscillations rather than planet-planet scattering (e.g., Takeda & Rasio 2005). Distinguishing between the two scenarios would make us understand the dynamical evolution of the eccentric giant planet CoRoT-10b.

Acknowledgements. The authors wish to thank the staff at ESO La Silla Observatory for their support and for their contribution to the success of the HARPS project and operation. The team at IAC acknowledges support by grant ESP2007-65480-C02-02 of the Spanish Ministerio de Ciencia e Innovación. The CoRoT/Exoplanet catalogue (Exodat) was made possible by observations collected for years at the Isaac Newton Telescope (INT), operated on the island of La Palma by the Isaac Newton group in the Spanish Observatorio del Roque de Los Muchachos of the Instituto de Astrophysica de Canarias. The German CoRoT team (TLS and University of Cologne) acknowledges DLR grants 50OW0204, 50OW0603, and 50QP0701. The French team wish to thank the Programme National de Planétologie (PNP) of CNRS/INSU and the French National Research Agency (ANR-08- JCJC-0102-01) for their continuous support for our planet search. The Swiss team acknowledges the ESA PRODEX programme and the Swiss National Science Foundation for their continuous support of the CoRoT ground follow-up. A. S. Bonomo acknowledges CNRS/CNES grant 07/0879-Corot. S. Aigrain acknowledges STFC grant ST/G002266. M. Gillon acknowledges support from the Belgian Science Policy Office in the form of a Return Grant.

References

Aigrain, S., Collier Cameron, A., Ollivier, M., et al. 2008, A&A, 488, L43
Alonso, R., Auvergne, M., Baglin, A., et al. 2008a, A&A, 482, L21
Alonso, R., Barbieri, M., Rabus, M., et al. 2008b, A&A, 487, L5
Auvergne, M., Bodin, P., Boisnard, L., et al. 2009, A&A, 506, 411
Baglin, A. 2003, Adv. Sp. Res., 31, 345
Bakos, G., Á., Kovács, G., Torres, G., et al. 2007, ApJ, 670, 826
Bakos, G. Á., Torres, G., Pál, A., et al. 2010, ApJ, 710, 1724
Baraffe, I., Chabrier, G., & Barman, T. 2008, A&A, 482, 315
Baranne, A., Queloz, D., Mayor, M., et al. 1994, A&AS, 119, 373
Barbieri, M., Alonso, R., Laughlin, G., et al. 2007, A&A, 476, L13
Barbieri, M., Alonso, R., Desidera, S., et al. 2009, A&A, 503, 601
Barge, P., Baglin, A., Auvergne, M., et al. 2008, A&A, 482, L17
Bean, J. L., Benedict, G. F., Charbonneau, D., et al. 2008, A&A, 486, 1039
Bessel, M. S., & Brett, J. M. 1988, PASP, 100, 1134

Bordé, P., Bouchy, F., Deleuil, M., et al. 2010, A&A, (Paper XI)
Bouchy, F., Moutou, C., Queloz, D., et al. 2008, in Transiting Planets, Proc. IAU Symp., 253, 129
Bruntt, H. 2009, A&A, 506, 235
Cabrera, J., Fridlund, M., Ollivier, M., et al. 2009, A&A, 506, 501
Chatterjee, S., Ford, E. B., Matsumura, S., & Rasio, F. A. 2008, ApJ, 685, 580
Cox, A. N. 2000, Allen's Astrophysical Quantities
Deeg, H., Gillon, M., Shporer, A., et al. 2009, A&A, 506, 343
Deeg, H., Moutou, C., Erikson, A., et al. 2010, Nature, 464, 384
Deleuil, M., Deeg, H. J., Alonso, R., et al. 2008, A&A, 491, 889
Deleuil, M., Meunier, J. C., Moutou, C., et al. 2009, AJ, 138, 649
Fridlund, M., Hébrard, G., Alonso, R., et al. 2010, A&A, 512, A14
Gillon, M., Pont, F., Demory, B.-O., et al. 2007a, A&A, 472, L13
Gillon, M., Demory B.-O., Barman, T., et al. 2007b, A&A, 471, L51
Giménez, A. 2006, A&A, 450, 1231
Giménez, A. 2009, in The Eighth Pacific Rim Conference on Stellar Astrophysics: a Tribute to Kam Ching Leung, ed. B. Soonthornthum, S. Komonjinda, K. S. Cheng, & K. C. Leung (San Francisco: ASP), 450, 291
Giménez, A., & Garcia-Pelayo, J. M. 1983, Ap&SS, 92, 203
Guillot, T., & Morel, P. 1995, A&AS, 109, 109
Guillot, T. 2005, Annual Review of Earth and Planetary Sciences, 33, 493
Guillot, T. 2008, Physica Scripta Volume T, 130, 014023
Hébrard, G., Desert, M.-J., Díaz, R. F., et al. 2010, A&A, 516, A95
Hut, P. 1981, A&A, 99, 126
Ibgui, L., Burrows, A., & Spiegel, D. S. 2010, ApJ, 713, 751
Ikoma, M., Guillot, T., Genda, H., et al. 2006, ApJ, 650, 1150
Iro, N., & Deming, L. D. 2010, ApJ, 712, 218
Johns-Krull, C. M., McCullough, P. R., Burke, C. J., et al. 2008, ApJ, 677, 657
Kovács, G., Bakos, G. Á., Hartman, J. D., et al. 2010, ApJ, submitted [arXiv:1005.5300]
Kozai, Y. 1962, AJ, 67, 591
Lainey, V., Arlot, J.-E., Karatekin, Ö., & Van Hoolst, T. 2009, Nature, 459, 957
Langton, J., & Laughlin, G. 2007, ApJ, 657, L113
Lanza, A. F., Pagano, I., Leto, G., et al. 2009, A&A, 493, 193
Lanza, A. F., Bonomo, A. S., Moutou, C., et al. 2010, A&A, in press [arXiv:1005.3602]
Léger, A., Rouan, D., Schneider, J., et al. 2009, A&A, 506, 287
Marzari, F., & Weidenschilling, S. J. 2002, Icarus, 156, 570
Matsumura, S., Takeda, G., & Rasio, F. A., et al. 2008, ApJ, 686, L29
Mayor, M., Pepe, F., Queloz, D., et al. 2003, The Messenger, 114, 20
Morel, P., & Lebreton, Y. 2008, Ap&SS, 316, 61
Moutou, C., Bruntt, H., Guillot, T., et al. 2008, A&A, 488, L47
Moutou, C., Hébrard, G., Bouchy, F., et al. 2009, A&A, 498, L5
Pál, A., Bakos, G. Á., Torres, G., et al. 2010, MNRAS, 401, 2665
Pepe, F., Mayor, M., Galland, F., et al. 2002a, A&A, 388, 632
Pepe, F., Mayor, M., Rupprecht, G., et al. 2002b, Messenger, 110, 9
Press, W. H., Teukolsky, S. A., Vetterling, W. T., & Flannery, B. P. 1992, Numerical recipes in FORTRAN, The art of scientific computing (Cambridge: University Press), 2nd edn.
Queloz, D., Bouchy, F., Moutou, C., et al. 2009, A&A, 506, 303
Queloz, D., Anderson, D., Cameron, A. C., et al. 2010, A&A, 517, L1
Rauer, H., Queloz, D., Csizmadia, S., et al. 2009, A&A, 506, 281
Recio-Blanco, A., Bijaoui, A., & de Laverny, P. 2006, MNRAS, 370, 141
Scargle, J. D. 1982, ApJ, 263, 835
Schlegel, D. J., Finkbeiner, D. P., & Davis, M. 1998, ApJ, 500, 525
Siess, L. 2006, A&A, 448, 717
Sing, D. K. 2010, A&A, 510, A21
Surace, C., Alonso, R., Barge, P., et al. 2008, in SPIE Conf., 7019
Takeda, G., & Rasio, F. A. 2005, ApJ, 627, 1001
Yoder, C. F., & Peale, S. J. 1981, Icarus, 47, 1
Winn, J. N., Holman, M. J., & Torres, G., et al. 2008, ApJ, 683, 1076
Winn, J. N., Howard, A. W., Johnson, J. A., et al. 2009, ApJ, 703, 2091

[1] Laboratoire d'Astrophysique de Marseille, Université Aix-Marseille & CNRS, 38 rue Frédéric Joliot-Curie, 13388 Marseille Cedex 13, France
e-mail: aldo.bonomo@oamp.fr
[2] Observatoire de l'Université de Genève, 51 chemin des Maillettes, 1290 Sauverny, Switzerland
[3] Observatoire de la Côte d' Azur, Laboratoire Cassiopée, BP 4229, 06304 Nice Cedex 4, France
[4] Department of Physics, Denys Wilkinson Building Keble Road, Oxford, OX1 3RH, UK
[5] LESIA, UMR 8109 CNRS, Observatoire de Paris, UVSQ, Université Paris-Diderot, 5 place J. Janssen, 92195 Meudon, France
[6] Institut d'Astrophysique Spatiale, Université Paris-Sud 11 & CNRS (UMR 8617), Bât. 121, 91405 Orsay, France
[7] Observatoire de Haute-Provence, Université Aix-Marseille & CNRS, 04870 St. Michel l'Observatoire, France
[8] Institut d'Astrophysique de Paris, UMR7095 CNRS, Université Pierre & Marie Curie, 98bis boulevard Arago, 75014 Paris, France
[9] Institute of Planetary Research, German Aerospace Centre, Rutherfordstrasse 2, 12489 Berlin, Germany
[10] Rheinisches Institut für Umweltforschung an der Universität zu Köln, Aachener Strasse 209, 50931 Köln, Germany
[11] Research and ScientiÞc Support Department, ESTEC/ESA, PO Box 299, 2200 AG Noordwijk, The Netherlands
[12] Instituto de AstrofÕsica de Canarias, 38205 La Laguna, Tenerife, Spain
[13] University of Vienna, Institute of Astronomy, Türkenschanzstr. 17, 1180 Vienna, Austria
[14] IAG, University of Sao Paulo, Brazil
[15] Thüringer Landessternwarte, Sternwarte 5, Tautenburg 5, 07778 Tautenburg, Germany
[16] University of Liège, Allée du 6 août 17, Sart Tilman, Liège 1, Belgium
[17] Space Research Institute, Austrian Academy of Science, Schmiedlstr. 6, 8042 Graz, Austria
[18] School of Physics and Astronomy, Raymond and Beverly Sackler Faculty of Exact Sciences, Tel Aviv University, Tel Aviv, Israel
[19] LUTH, Observatoire de Paris, CNRS, Université Paris Diderot; 5 place Jules Janssen, 92195 Meudon, France
[20] INAF, Osservatorio Astrofisico di Catania, via S. Sofia, 78, 95123 Catania, Italy
[21] Dipartimento di Astronomia, Università di Padova, 35122 Padova, Italy
[22] SUPA, School of Physics and Astronomy, University of St Andrews, Fife KY16 9SS
[23] Universität Bern Physics Inst, Sidlerstrasse 5, 3012 Bern, Switzerland
[24] Centre for Astronomy and Astrophysics, TU Berlin, Hardenbergstr. 36, 10623 Berlin, Germany